Hindawi
Mathematical Problems in Engineering
Volume 2018, Article ID 6132891, 10 pages
https://doi.org/10.1155/2018/6132891

Research Article

A Mathematical Model for Top Nutation Based on Inertial Forces of Distributed Masses

Ryspek Usubamatov and Albina Omorova

Kyrgyz State Technical University, Bishkek, Kyrgyzstan

Correspondence should be addressed to Ryspek Usubamatov; ryspek0701@yahoo.com

Received 8 June 2017; Revised 8 November 2017; Accepted 8 January 2018; Published 5 March 2018

Academic Editor: Filippo Cacace

The main property of gyroscopic devices is maintaining the axis of a spinning rotor, a mathematical model formulated on the principle of the change in the angular momentum. This principle is used for mathematical modeling of the motions of a top at known publications. Nevertheless, practical tests of gyroscopic devices do not correspond to this analytical approach. Recent investigations have demonstrated that the origin of gyroscope properties is more complex than that represented in known publications. The applied torque on a gyroscope produces internal torques of the spinning rotor based on the action of the several inertial forces. These forces are the centrifugal, Coriolis, and common inertial forces as well as the change in the angular momentum generated by the mass elements and center-mass of the spinning rotor. The action of these torques manifests itself in the resistance and precession torques of the gyroscopic devices. These inertial torques act simultaneously and interdependently around two axes and represent the fundamental principles of the gyroscope theory. The new inertial torques enable deriving mathematical models for the motions of well-known top that is the simplest form of gyroscopic devices. The novelty of the work is mathematical models for the motions of the top based on action of eight inertial forces acting around its two axes. The obtained mathematical models for the top nutation and self-stabilization are represented in terms of machine dynamics and vibration analysis. The new analytical approach for motions of the well-balanced top and top with eccentricity of the center-mass definitely responds to the practical results.

1. Introduction

L. Euler first laid out the mathematical foundations for the gyroscope theory in his work on the dynamics of rigid bodies back in 1765. Since Industrial Revolution time, I. Newton, J-L. Lagrange, L. Poinsot, J. L. R. D'Alembert, P-S. Laplace, L. Foucault, and other brilliant scientists have investigated, developed, and added new interpretations of the gyroscope effects, which are in full display in the rotor's persistence in maintaining its plane of rotation. The applied theory of gyroscopes emerged mainly in the twentieth century in numerous publications that described the gyroscope effects [1]. The gyroscope properties feature many engineering mechanisms and devices with rotating parts, which thus need to be computed for their proper functioning [2, 3]. Gyroscope effects are used in numerous gyroscopic devices in aerospace engineering, as well as on ships and other industries [4, 5]. The most basic textbooks of classical mechanics have chapters on the gyroscope theory [6, 7] and consider motions with vibrations analysis [8]. Numerous and valuable publications have dedicated themselves to gyroscope effects and their applications in engineering [9–12]. Intuitively and without mathematical models, some researchers have noted that, on a gyroscope, the inertial forces that manifest the gyroscope effects are acting. However, in known publications, mathematical models for the gyroscope effects do not seem to match their practical applications in gyroscopic devices [13–17]. Therefore, researches have spawned artificial terms such as gyroscope resistance and gyroscope couple, as well as fantastical properties that contradict rules of classical mechanics. It is for this reason that the gyroscope theory still attracts many researchers who seek to discover true gyroscope theory [16, 18].

Mechanically, a gyroscope is a spinning disc in which the axle is free to assume any orientation. The simplest gyroscope is represented by a top toy that is one of the most remarkable and widely recognized toys in the world. They still attract attention through their astonishing behavior and

Table 1: Internal torques acting on a gyroscope.

Type of a torque generated by	Equation (N·m)
Centrifugal forces, $T_{\mathrm{ct}.i}$ Inertial forces, $T_{\mathrm{in}.i}$	$T_{\mathrm{ct}.i} = T_{\mathrm{in}.i} = 2\left(\frac{\pi}{3}\right)^2 J\omega\omega_i$
Coriolis forces, $T_{\mathrm{cr}.i}$	$T_{\mathrm{cr}.i} = \left(\frac{8}{9}\right) J\omega\omega_i$
Change in an angular momentum, $T_{\mathrm{am}.i}$	$T_{\mathrm{am}.i} = J\omega\omega_i$
Resistance torque, $T_{r.i} = T_{\mathrm{ct}.i} + T_{\mathrm{cr}.i}$	$T_{r.i} = \left[2\left(\frac{\pi}{3}\right)^2 + \frac{8}{9}\right] J\omega\omega_i$
Precession torque, $T_{p.i} = T_{\mathrm{in}.i} + T_{\mathrm{am}.i}$	$T_{p.i} = \left[2\left(\frac{\pi}{3}\right)^2 + 1\right] J\omega\omega_i$

unusual gyroscopic properties. The motions of top toy have been described analytically in numerous publications and with complex numerical modeling [19] based on Lagrangian dynamics on Euler coordinates that are solved with computer software [20].

However, all publications contain approximations, assumptions, and simplifications and explain gyroscope effects by the physical principle of the spinning rotor's angular momentum that generates the precession torque and motions. Gyroscope effects still represent a problem that remains to be solved. The origin of gyroscope effects is more complex than those represented in the theories known to date. Recent investigations into the physical principles of gyroscope motions demonstrate four classical inertial forces acting upon a spinning rotor to generate the gyroscope effects. Research shows that centrifugal, common inertial, and Coriolis forces, in addition to change in the angular momentum of spinning rotors, are the basis for all gyroscope effects and properties [21–24]. Applied to the gyroscope, an external torque generates several torques based on the action of the aforementioned forces. In turn, the centrifugal and Coriolis forces of the rotating mass elements generate a resistance torque that counteracts the inclination of the rotor's location. Common inertial forces, rotating mass elements, and change in the angular momentum of a spinning rotor generate a precession torque. All torques are interrelated and occur simultaneously. New mathematical models for acting torques accurately describe the physics of gyroscope effects and are validated by tests [21]. Table 1 represents four different torques generated by the inertial forces of the mass elements and center-mass of the spinning rotor under the action of the external torque that was applied to the gyroscope. The action of these torques should be considered for mathematical models of the gyroscopic devices and the top's motions and nutation.

In Table 1, $T_{r.i}$ is a resistance torque generated by the centrifugal ($T_{\mathrm{ct}.i}$) and Coriolis ($T_{\mathrm{cr}.i}$) forces acting around axis i; $J = (mR^2/2)$ is the mass moment of inertia of the disc around axis ox or oy [6]; $T_{p.i}$ is a precession torque generated by the common inertial forces ($T_{\mathrm{in}.i}$) and change in the angular momentum ($T_{\mathrm{am}.i}$) acting around axis i; and ω is the angular velocity of a spinning rotor.

When applied to a gyroscope, an external torque generates angular velocities of precessions around two axes and activates simultaneously and interdependently eight internal torques. The equations of these torques (Table 1) demonstrate that the centrifugal, common inertial, and Coriolis forces of the spinning rotor are real active physical components, just like the change in the angular momentum. The new equations for the internal torques demonstrate their proportional dependence on a rotor's mass moment of inertia and angular velocity of the spinning rotor, as well as on the angular velocity of its precession. New mathematical models for these torques clearly describe the physics of gyroscope properties and explain the unusual motions of gyroscopic devices. The aim of this paper is to represent mathematical models for the motions of the well-balanced top and with its eccentricity of the center-mass. This analytical approach is based on the action of centrifugal, common inertial, and Coriolis forces as well as the change in the angular momentum generated by the mass elements and center-mass of a spinning rotor. New mathematical model for the top motions describes the physics of forces acting on the top and its motions that represents the novelty of the work. The obtained mathematical models for top nutation and self-stabilization are represented in terms of machine dynamics and vibration analysis.

2. Materials and Methods

The new mathematical models for gyroscope motions will consider the simultaneous and interdependent actions of internal torques (Table 1). The external load torque generates eight internal resistance and precession torques acting around two axes and reveals new gyroscope properties [21]. The interdependent action of internal torques is used to model the behavior of different gyroscopic devices, including the simplest top.

Observation of a fast-spinning top shows that it preserves the vertical position of the axis, remains steady on the supporting pivot, and avoids tilting or falling to the ground. If the axis of a spinning top toy is inclined from the vertical axis under the action of an external torque, the axis starts to describe the vertical circular cone of the precessed motion. Then the spinning top stabilizes itself and its spin axis goes to a vertical position.

However, the axis of a spinning top has free oscillation of the periodic complex motion, which is called nutation, and reveals itself as fast shivering of the precessing axis. This phenomenon of the top's gyroscope nutation represents small but fast oscillations of the spinning rotor's axis at about its mean position. The nature of gyroscope nutation is represented by the following sources: the center-mass is displaced from the axis of rotation, the shocked displacement of the center-mass is generated by the action of an external force and the imperfect surface geometry of the tip of the top's leg, and so forth.

The action of the center-mass, having been displaced from the spinning top, represents the continuing existence of a disturbing force that generates a forced oscillation. Any free oscillation of the spinning top is connected with an angular acceleration that eventually ceases because of a loss of energy. The amplitudes of free oscillated motions are very small in the case of a rapidly rotating top. Because of the inevitable presence of resistances, these oscillations for a

well-balanced top toy are subject to asymptotically rapid decay. In most cases, the nutation of a well-balanced top toy is quickly damped by the action of inertial resistance forces and friction forces in the bearing, leaving uniform precession.

Gyroscopes with a high angular velocity represent over-damped or critically damped systems according to the theory of vibration [8]. This makes it possible to neglect nutation in solving most engineering problems and to formulate a gyroscope theory that takes into account only the precessions. However, for a gyroscope with low angular velocity, nutation is a regular process and represents a simple damped system.

The nutation process of the top can be considered in terms of machine dynamics, particularly in terms of vibration analysis [8]. The acting forces on the top are its weight and the force generated by centrifugal forces of the top toy's center-mass, torques generated by the inertial forces of the rotating mass elements, and change in the angular momentum. The simulation of a free nutation process is presented by modeling it with a damping process and energy losses in the oscillation of a not so well-balanced spinning top.

Vibration analysis often takes into account the energy losses by means of a single factor called the damping factor. The nutation model of the spinning top consists of a not so well-balanced mass and a damper that represents the action of the top's weight and several internal torques. In the case of a gyroscope's free nutation process, the action of the single shock type torque on a spinning top toy represents one period of an oscillation with a short time for a single cycle. The damping resistance torques decay the action of one shock torque, resulting in the inclination of only the spinning top's axis. For well-balanced gyroscopic devices and a top with high angular velocities, the process of the damped oscillation is not displayed.

For a top that possesses an eccentric rotating mass, that is, the center-mass being displaced on some small distance from the top's axis, nutation is a regular process. The centrifugal force of the offset mass is asymmetric, which causes an angular displacement of the top's shaft. The spinning top toy is constantly being displaced and moved by these asymmetric forces. The eccentric rotating mass of the top represents harmonic nutation, which means that the top is forced to nutate at the frequency of excitation [8]. A plot using the nutation amplitude along one axis and the forcing frequency along the other axis is then described as a performance or response curve for the system. The eccentric rotation of the mass at about the top's axis is modeled as a sinusoidal wave, as shown in Figure 1. Here, the function $y = e \sin \alpha$ denotes the displacement of the eccentric mass that represents the excitation input, where e is the eccentricity of mass location. The frequency of this sine wave is also the frequency at which nutation occurs.

The analysis of a gyroscope motions and nutation is conducted using the example of a top that is not well balanced and is thus tilted (Figure 2). The motions of the spinning top are considered at around the point of support O. If the axis of a top is adjusted on the angle γ to the horizontal position and released, then, under the influence of the force of gravity, its axis should tilt in the direction of the action of this force.

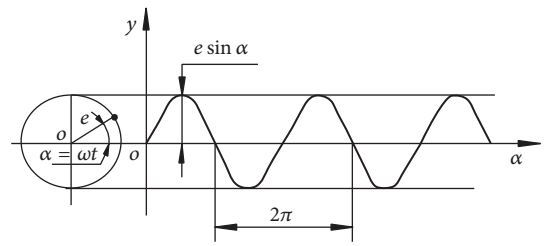

Figure 1: The position of a top's eccentric motion according to sinusoidal law.

As a result, the top's axis will begin to precess at about the vertical and horizontal positions. The precessions of the top are also accompanied by visually undetectable nutational oscillations, which decay rapidly according to the action of the internal torques. Because of the internal torques' resistance forces, the proper rotation of the top gradually slows down, while the precession velocities correspondingly increase. When the angular velocity of the top becomes smaller, the resistance forces of the internal torques become weaker, and the top becomes unstable and falls. In the case of a slowly rotating top, the nutational oscillations are noticeable and manifest a substantial change in the pattern of the top toy's axial movement. In this case, the end of the top's axis can describe a clearly visible wavy or looped curve alternately departing from the vertical position. In the case of a highly rotating top, the nutational oscillations can decrease and manifest the stabilization of the top's axial movement. The top's axis can approach the vertical position.

The motions of a not so well-balanced spinning top are complex. The equation of nutation is formulated by the action of several forces on the top. These forces represent the top's weight, the centrifugal forces of eccentric mass and center-mass, the centrifugal and Coriolis forces generated by the rotating mass elements, the common inertial forces, and the rate of change in the angular momentum of the spinning toy. These forces produce the torques acting on the top. These are demonstrated in Figure 2 and formulated by the equations presented in Table 1.

The centrifugal force of the eccentric mass generates the variable torque represented by the following equation [7]:

$$T_{ex} = \pm F * l = \pm me\omega^2 l \sin \alpha \quad \text{by axis } ox, \tag{1}$$

$$T_{ey} = \pm F * l = \pm me\omega^2 l \cos \gamma \cos \alpha \quad \text{by axis } oy, \tag{2}$$

where $F = me\omega^2$ is the centrifugal force generated by the rotated eccentric mass m, l is the length of the top's leg, γ is the tilt angle of the top's axis, α is the angle that should be used for calculating the maximum magnitude, and T_{ex} and T_{ey} are the torques acting around axes ox and oy, respectively.

The weight of a top generates torque, for which the equation is as follows: $T = W * l = mgl \cos \gamma$. $T_{\text{ct.}my}$ is the torque generated by the centrifugal force of the rotating top's center-mass m around axis oy. Other acting torques are presented in Table 1.

The parameters defined above allow for the formulation of a mathematical model for a top's motion around axes ox

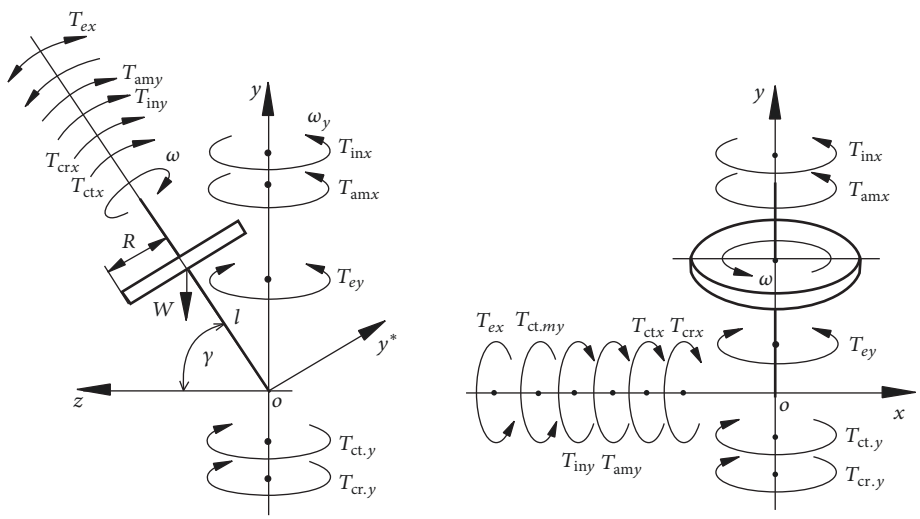

Figure 2: Forces acting on a spinning top.

and oy in Euler's form. The torques acting on the top are similar to torques acting on the gyroscope suspended from a flexible cord [22, 23]. Both models consider the gyroscope with one-side support to be equal except for the added torque generated by the centrifugal force of the eccentric rotating center-mass. As such, the mathematical model for a top's motion around axes ox and oy is represented by the following system of equations:

$$J_x \frac{d\omega_x}{dt} = T + T_{\mathrm{ct}.my} \pm T_{ex} - T_{\mathrm{ct}x} - T_{\mathrm{cr}x} - T_{\mathrm{in}y} \cos\gamma - T_{\mathrm{am}y} \cos\gamma, \tag{3}$$

$$J_y \frac{d\omega_y}{dt} = \left(\pm T_{ey} + T_{\mathrm{in}x} + T_{\mathrm{am}x} - T_{\mathrm{ct}y} - T_{\mathrm{cr}y}\right) \cos\gamma, \tag{4}$$

where $J_i = (mR^2/4) + ml^2$ is the top's mass moment of inertia around axis i [6], while the sign ($\pm$) denotes (+) and (−) as the positive and negative directions of the action, respectively, for the torque generated by the eccentric mass.

The torques generated by the centrifugal forces of the rotating top's center-mass around axis oy are defined by the following equation:

$$T_{\mathrm{ct}.my} = F_{\mathrm{ct}.my} l \sin\gamma = ml \cos\gamma {\omega_y}^2 l \sin\gamma = ml^2 \cos\gamma \sin\gamma {\omega_y}^2, \tag{5}$$

where $F_{\mathrm{ct}.my} = ml \cos {\omega_y}^2$ is the centrifugal force of the top's center-mass rotating around axis oy and ω_y is the angular velocity of the top around axis oy; the other components are as specified above.

The methodology towards a solution for (3) and (4) by adding the ratio of the angular velocities of a gyroscope around axes $\omega_y = f(\omega_x)$ is presented in Usubamatov [22, 23]. Substituting the defined parameters ((1), (2), and (5) and Table 1) into (3) and (4), transformation yields the equations of the top's motions as follows:

$$J_x \frac{d\omega_x}{dt} = mgl \cos\gamma + ml^2 \sin\gamma \cos\gamma \omega_y^2 \pm me\omega^2 l \sin\alpha - \left[2\left(\frac{\pi}{3}\right)^2 + \frac{8}{9}\right] J\omega\omega_x - J\omega\omega_y \cos\gamma, \tag{6}$$

$$J_y \frac{d\omega_y}{dt} = \left[\pm me\omega^2 l \cos\alpha + \left\{2\left(\frac{\pi}{3}\right)^2 + 1\right\} J\omega\omega_x - \frac{8}{9} J\omega\omega_y\right] \cos\gamma, \tag{7}$$

$$\omega_y = -\left(\frac{2\pi^2 + 8}{\cos\gamma} + 2\pi^2 + 9\right)\omega_x, \tag{8}$$

where all parameters are as specified above.

Solving (6), (7), and (8) yields the maximum and minimum angular precessions ω_x and ω_y which allow for defining the nutation amplitudes around axes ox and oy, respectively. Changes in the angular velocities of precessions around two axes make it possible to depict the trajectory of a top's center-mass nutation. The mathematical model for the motions of a tilted top is derived from (6), (7), and (8). Substituting the expression ω_y from (8) into (6), transformation yields the following equation:

$$J_x \frac{d\omega_x}{dt} = mgl \cos\gamma + ml^2 \tan\gamma \left(2\pi^2 + 8 + \left[2\pi^2 + 9\right] \cos\gamma\right)^2 \omega_x^2 \pm me\omega^2 l \sin\alpha - \left[2\left(\frac{\pi}{3}\right)^2 + \frac{8}{9}\right] J\omega\omega_x - \left(2\pi^2 + 8 + \left[2\pi^2 + 9\right] \cos\gamma\right) J\omega\omega_x, \tag{9}$$

where all parameters are as specified above.

Table 2: Technical data of a top.

Parameter	Data
Angular velocity, ω	2000 rpm
Radius of the disc, R	0.025 m
Length of the leg, l	0.02 m
Eccentricity of the centre mass, e	0.0001 m
Angle of tilt, γ	75.0°
Weight, W	0.02 kg
Mass moment of inertia, kgm^2	
Around axis oz,$J = mR^2/2$	0.625×10^{-5}
Around axes ox and oy of the centre mass, $J = mR^2/4$	0.3125×10^{-5}
Around axes ox and oy at the point of support,$J_x = J_y = mR^2/4 + ml^2$	1.1125×10^{-5}

Self-Stabilization. The practical observation of a tilted, well-balanced spinning top with a high angular velocity proves its capacity for self-stabilization. The axis of the tilted spinning top goes to the vertical position by the action of the internal torques, whose magnitudes are bigger than torques generated by the top's weight. The necessary condition for a top's self-stabilization is formulated in the following approaches. The expression of the variable torque generated by the eccentric mass is omitted from (9). The torques generated by the top's weight and by the centrifugal forces of the rotating top's center-mass around axis oy are acting in an anticlockwise direction. By contrast, the torques based on the action of the centrifugal and Coriolis forces as well as the factored change in the angular momentum are acting in a clockwise direction. The torques acting in a clockwise direction account for the self-stabilization of the top, as expressed in the following equation:

$$\begin{aligned} &ml\left\{g\cos\gamma + l\tan\gamma\left(2\pi^2 + 8 + \left[2\pi^2 + 9\right]\cos\gamma\right)^2\omega_x^2\right\} \\ &\quad = \left[2\left(\frac{\pi}{3}\right)^2 + \frac{8}{9}\right]J\omega\omega_x \\ &\qquad + \left(2\pi^2 + 8 + \left[2\pi^2 + 9\right]\cos\gamma\right)J\omega\omega_x. \end{aligned} \tag{10}$$

Analysis of (10) shows that equilibrium of the acting torques depends on two main components, that is, the angular velocity of the top and the angle of its inclination. The angular velocity of precession depends on the first one. The stabilization process is intensive when the radius of gyration and angular velocity of spinning both have big value in addition to the length of the top's leg being short, that is, the center-mass of the top is located towards the lower part. These components explain the unstable spinning of a top and other spinning objects with a long leg and small radius. This property is confirmed by ordinary tests. A detailed analysis of (10) demonstrates that the magnitude of its right component is always bigger than its left one except for the very low value of the top's angular velocity that does not support its rotation. This top property is validated by practical observation. The low critical angular velocity of the top, which leads to a loss of self-stabilization, is defined when both the right and left sides of (10) are equal.

3. Working Example

The example considers the nutation process of a disc-type top whose data is presented in Table 2, whose formulas of the mass moment of inertia are represented in Hibbeler [6]. The center-mass of the top is located at the plane of the disc (Figure 2). The top initially possesses a displaced mass, while spinning around a vertical axis is conducted with nutation.

The torque generated by the top's weight is as follows:

$$\begin{aligned} T &= mgl\cos\gamma = 0.02 \times 9.81 \times 0.02\cos 75.0^\circ \\ &= 1.015605932 \times 10^{-3}\ \text{Nm}. \end{aligned} \tag{11}$$

The torque generated by the centrifugal force of the top's center-mass rotation around axis oy is as follows:

$$\begin{aligned} T_{\text{ct}.my} &= ml\cos\gamma\omega_y^2 l\sin\gamma \\ &= 0.02 \times 0.02 \times \cos 75^\circ \\ &\quad \times \left(\frac{2\pi^2 + 8}{\cos 75^\circ} + 2\pi^2 + 9\right)^2 \omega_x^2 0.02\sin 75^\circ \\ &= 0.036945927\omega_x^2\ \text{Nm}. \end{aligned} \tag{12}$$

The maximal torque generated by the centrifugal forces of the eccentric rotating center-mass around axis ox is as follows:

$$\begin{aligned} T_{ex} &= \pm me\omega^2 l\sin\alpha \\ &= \pm 0.02 \times 0.0001 \times \left(2000 \times \frac{2\pi}{60}\right)^2 0.02\sin 90.0^\circ \\ &= \pm 1.752817777 \times 10^{-3}\ \text{Nm}, \end{aligned} \tag{13}$$

where all parameters are as specified above.

Substituting the defined parameters (Table 2, (11), (12)) into (9), transformation yields the following differential equation:

$$\begin{aligned} 1.1125 \times 10^{-5}\frac{d\omega_x}{dt} &= 1.015605932 \times 10^{-3} \\ &\quad + 0.0369459275\omega_x^2 \end{aligned}$$

$$\begin{aligned}
&\pm 1.752817777 \times 10^{-3} \\
&- \left[2\left(\frac{\pi}{3}\right)^2 + \frac{8}{9}\right] \times 0.625 \\
&\times 10^{-5} \times 2000\left(\frac{2\pi}{60}\right)\omega_x \\
&- \left(2\pi^2 + 8 + \left[2\pi^2 + 9\right]\cos 75^\circ\right) \\
&\times 0.625 \times 10^{-5} \\
&\times 2000\left(\frac{2\pi}{60}\right)\omega_x.
\end{aligned} \tag{14}$$

Simplification and transformation of (14) yield the following equation:

$$\begin{aligned}
&3.011157318 \times 10^{-4}\frac{d\omega_x}{dt} \\
&\quad = 0.027488981 \pm 0.047442787 - 1.354853169\omega_x \\
&\quad + \omega_x^2.
\end{aligned} \tag{15}$$

Separation of variables and transformation for the differential equation (15) yield the following expression:

$$\begin{aligned}
&\frac{d\omega_x}{\omega_x^2 - 1.354853169\omega_x + 0.027488981 \pm 0.047442787} \\
&\quad = 3320.982248327dt.
\end{aligned} \tag{16}$$

The denominator on the left side of (16) is represented by an equation with a known solution:

$$\omega_x^2 - a\omega_x + b = 0, \tag{17}$$

where the solutions are $\omega_x = a/2 \pm \sqrt{(a/2)^2 - b}$ and yield the following results: $a = 1.354853169$, $b = 0.047442787(0.579413283 \pm 1)$.

Substituting the new expressions into (16) and then converting to integral forms with definite limits yield the following expression:

$$\begin{aligned}
&\int_0^{\omega_x} \frac{d\omega_x}{\left(\omega_x - a/2 + \sqrt{(a/2)^2 - b}\right) \times \left(\omega_x - a/2 - \sqrt{(a/2)^2 - b}\right)} \\
&\quad = 3320.982248327\int_0^t dt.
\end{aligned} \tag{18}$$

Integral equation (18) is transformed and represented by the following equation:

$$\begin{aligned}
&-\frac{1}{2\sqrt{(a/2)^2 - b}}\int_0^{\omega_x}\left[\frac{1}{\left(\omega_x - a/2 + \sqrt{(a/2)^2 - b}\right)}\right. \\
&\left. - \frac{1}{\left(\omega_x - a/2 - \sqrt{(a/2)^2 - b}\right)}\right]d\omega_x \\
&\quad = 3320.982248327\int_0^t dt.
\end{aligned} \tag{19}$$

Left integral of (19) is tabulated and presents integral $\int(dx/(x-a)) = \ln|a-x| + C$. Right integral is simple, and finally integrals have the following solution:

$$\begin{aligned}
&\ln\left(\omega_x - \frac{a}{2} + \sqrt{\left(\frac{a}{2}\right)^2 - b}\right)\Bigg|_0^{\omega_x} \\
&\quad - \ln\left(\omega_x - \frac{a}{2} - \sqrt{\left(\frac{a}{2}\right)^2 - b}\right)\Bigg|_0^{\omega_x} \\
&\quad = -\left(6641.964496654\sqrt{\left(\frac{a}{2}\right)^2 - b}\right)t\Bigg|_0^t
\end{aligned} \tag{20}$$

giving rise to the following:

$$\begin{aligned}
&\ln\left(\frac{\omega_x - a/2 + \sqrt{(a/2)^2 - b}}{-a/2 + \sqrt{(a/2)^2 - b}}\right) \\
&\quad - \ln\left(\frac{\omega_x - a/2 - \sqrt{(a/2)^2 - b}}{-a/2 - \sqrt{(a/2)^2 - b}}\right) \\
&\quad = -\left(6641.964496654\sqrt{\left(\frac{a}{2}\right)^2 - b}\right)t.
\end{aligned} \tag{21}$$

The next transformation yields the following result:

$$\begin{aligned}
&\frac{\left[\omega_x - a/2 + \sqrt{(a/2)^2 - b}\right] \times \left[-a/2 - \sqrt{(a/2)^2 - b}\right]}{\left[\omega_x - a/2 - \sqrt{(a/2)^2 - b}\right] \times \left[-a/2 + \sqrt{(a/2)^2 - b}\right]} \\
&\quad = e^{-(6641.964496654 \times \sqrt{(a/2)^2 - b})t}.
\end{aligned} \tag{22}$$

The right component of (22) has small value of a high order that can be neglected. Substituting expressions a and b into simplified equation (22), transformation yields the following result:

$$\begin{aligned}
\omega_x &= \frac{1.354853169}{2} \\
&\quad - \sqrt{\left(\frac{1.354853169}{2}\right)^2 - 0.047442787\,(0.579413283 \pm 1)} \\
&= 0.677426584 \\
&\quad - 0.217813652\sqrt{9.672846089 - (0.579413297 \pm 1)}.
\end{aligned} \tag{23}$$

Solving (23) yields the maximal and minimal value of the precession angular velocity for the gyroscope around axis ox:

$$\omega_{x.\max} = +0.0577694142 \text{ rad/s}, \quad \omega_{x.\min} = -0.0145709463 \text{ rad/s}, \tag{24}$$

where the signs (+) and (−) represent motion in an anticlockwise and clockwise direction around axis ox, respectively.

Equation (24) enables the angular velocity of a well-balanced top precession around axes ox and oy to be defined, as represented by the following magnitudes:

$$\omega_x = 0.020602562 \text{ rad/s}, \tag{25}$$

$$\omega_y = \left(\frac{2\pi^2 + 8}{\cos 75^\circ} + 2\pi^2 + 9\right)\omega_x = 2.800203014 \text{ rad/s}. \tag{26}$$

The precession's linear velocities of a balanced top's center-mass around axes ox and oy have the following magnitudes:

$$V_x = \omega_x l \cos\gamma = 0.020602562 \times 20 \cos 75.0^\circ = 0.106646708 \text{ mm/s}, \tag{27}$$

$$V_y = \omega_y l \cos\gamma = 2.800203014 \times 20 \cos 75.0^\circ = 14.494917406 \text{ mm/s}. \tag{28}$$

The distance of precessed motion for the center-mass of a balanced top per nutation of half oscillation time is as follows:

$$a_x = V_y t = 14.494917406 \times 0.015 = 0.217 \text{ mm}. \tag{29}$$

The maximal and minimal value of the linear velocity of the top's center-mass around axis ox have the following magnitudes:

$$V_{x\max} = \omega_{x\max} l = 0.0577694142 \times 20 \cos 75^\circ = -0.2990 \text{ mm/s}, \quad V_{x\min} = \omega_{x\min} l = 0.0145709463 \times 20 \cos 75^\circ = +0.0754 \text{ mm/s}, \tag{30}$$

where the signs (−) and (+) represent linear velocity in negative and positive direction along axis oy, respectively.

The time spent on a half oscillation is as follows:

$$t = \frac{\pi}{n} = \frac{\pi}{2000 \times 2\pi/60} = 0.015 \text{ s}. \tag{31}$$

The maximal and minimal value of the amplitudes of center-mass nutation around axis ox as well as the location of a balanced top are as follows:

$$a_{y\max} = V_{x\max} t = 0.2990 \times 0.015 = -0.0044 \text{ mm}, \quad a_{y\min} = V_{x\min} t = -0.0754 \times 0.015 = +0.0011 \text{ mm}, \quad a_y = V_x t = 0.1066 \times 0.015 = 0.0016 \text{ mm}. \tag{32}$$

The total amplitude of oscillation around axis ox is as follows:

$$a_y = |a_{y\max}| + a_{y\min} = 0.0044 + 0.0011 = 0.0055 \text{ mm}. \tag{33}$$

The maximal and minimal value of the angular velocity for top's precession around axis oy are defined by (8). Substituting the parameters defined above and in Table 2 into (26), transformation yields the following results:

$$\omega_{y.\max} = \left(\frac{2\pi^2 + 8}{\cos\gamma} + 2\pi^2 + 9\right)\omega_{x.\max} = \left(\frac{2\pi^2 + 8}{\cos 75^\circ} + 2\pi^2 + 9\right)0.0577694142 = +7.851746194 \text{ rad/s}, \tag{34}$$

$$\omega_{y.\min} = \left(\frac{2\pi^2 + 8}{\cos\gamma} + 2\pi^2 + 9\right)\omega_{x.\min} = \left(\frac{2\pi^2 + 8}{\cos 75^\circ} + 2\pi^2 + 9\right)(-0.0145709463) = -1.980414277 \text{ rad/s}, \tag{35}$$

where the signs (+) and (−) represent motion in an anticlockwise and clockwise direction around axis oy, respectively.

The maximal and minimal value of the linear velocities of the top center-mass around axis oy indicate the following magnitudes:

$$V_{y\max} = \omega_{y\max} l \cos\gamma = 7.851746194 \times 20 \cos 75.0^\circ = +40.643629046 \text{ mm/s}, \quad V_{y\min} = \omega_{y\min} l \cos\gamma = -1.980414277 \times 20 \cos 75.0^\circ = -10.251378643 \text{ mm/s}, \tag{36}$$

where the signs (+) and (−) represent linear velocity in positive and negative direction along axis ox, respectively.

The maximal and minimal value of the amplitudes of the center-mass nutation around oy as well as the location of a balanced top (29) are as follows:

$$a_{x\max} = V_{y\max} t = 40.643629046 \times 0.015 = +0.6096 \text{ mm}, \quad a_{x\min} = V_{y\min} t = -10.251378643 \times 0.015 = -0.1537 \text{ mm}. \tag{37}$$

The total amplitude of oscillation around axis oy is as follows:

$$a_{xt} = a_{x\max} + |a_{x\min}| = 0.6096 + 0.1537 = 0.7633 \text{ mm}. \tag{38}$$

The positive and negative values of the angular velocities around axes ox and oy ((34) and (35)), respectively, mean

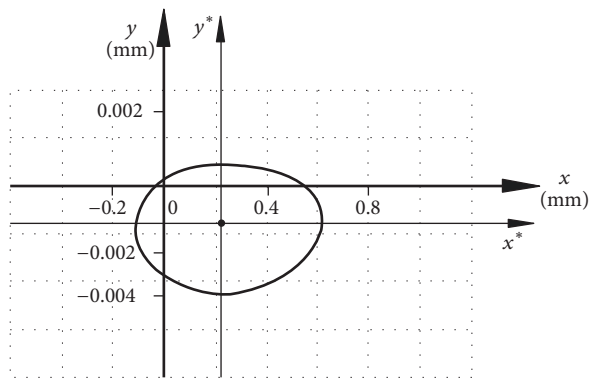

Figure 3: Nutation's amplitudes of top's center-mass.

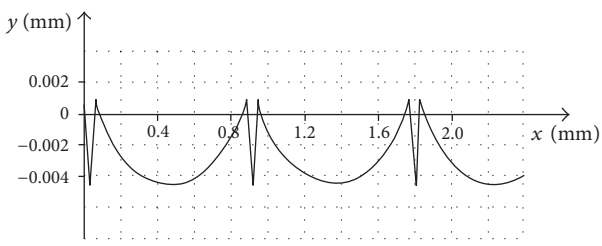

Figure 4: Deployed diagram of top's nutation.

rotation in anticlockwise and clockwise directions. Hence, the linear motions of the top's center-mass will be in negative and positive directions along the axes. This situation is expressed in the diagrams of nutation amplitudes.

This diagram of the top's nutation loop is presented in Figure 3 and contains two coordinate systems. The system with asterisks is accepted for the motions of a balanced top. The figure demonstrates that the actual loop of amplitudes for top's center-mass has stretched down along the axis oy. This is a natural result, because any action of the centrifugal force in the direction of top toy's weight increases the amplitude. Any action in the opposite direction decreases the amplitude of nutation.

The magnitudes of precessed motion's distance (29) and the amplitudes of oscillations around axes ox (37) and oy (32) make it possible for diagrams of top's nutation to be depicted. The distance of the center-mass's motion along axes oy and ox is bigger than the minimal value of the amplitude. It means that the deployed diagram of top's nutation does not have loops of oscillated motions. The following represent the half-cyclic nutation of top along the axis ox:

$$\begin{aligned} a_{xc.\max} &= a_x + a_{x.\max} = 0.217 + 0.609 = 0.826\,\text{mm}, \\ a_{xc.\min} &= a_x - a_{x.\min} = 0.217 - 0.153 = 0.064\,\text{mm}. \end{aligned} \tag{39}$$

Deployed diagram of top's nutation (illustrated in Figure 4).

The deployed diagram of top's nutation can have loops if the negative amplitude of oscillation along axis ox is bigger than the distance of top's motion for the same precessing time. Equations of top's motions with the given and calculated data of nutation parameters demonstrate that the amplitude and frequency of nutation are cyclic. The cycles are different, because the centrifugal force of top's eccentric center-mass acts at the first semicircle of rotation in the direction of precessed motions and at the second semicircle in a direction opposite to that of the precessed motions. The result of this example demonstrates that the axis of a spinning top toy precesses with a rapid tremor of small amplitude. For top with a big, eccentric, rotating center-mass, the tremor can be visible; however, for small eccentrics, this can hardly be noticeable to the naked eye.

Self-Stabilization. The presented data of a tilted spinning top allow the condition for its self-stabilization to be checked. To make it simple, this is considered a well-balanced top that does not have the eccentric mass. Substituting the data defined above and in Table 2 into (10), transformation yields the following result:

$$\begin{aligned} &2 \times 0.02 \left[9.81 \cos 75^\circ + 0.02 \tan 75^\circ \right. \\ &\quad \left. \times \left(2\pi^2 + 8 + \left[2\pi^2 + 9\right] \cos 75^\circ\right)^2 0.020602562^2 \right] \\ &\quad = \left\{ \left[2\left(\frac{\pi}{3}\right)^2 + \frac{8}{9} \right] + 2\pi^2 + 8 + \left[2\pi^2 + 9\right] \cos 75^\circ \right\} \\ &\quad \times 0.025^2 \times 2000 \left(\frac{2\pi}{60}\right) 0.020602562 \end{aligned} \tag{40}$$

or $0.10313000 < 0.1031808$.

The right component is bigger than the left one, that is, the top stabilizes itself.

4. Results

The simplest form of a gyroscope is a top, whose motions are described by known publications in terms of mathematical models based on the change in the angular momentum. The analytical study of forces acting on a well-balanced top and on a top toy with the eccentricity of center-mass has formulated new mathematical models for its motions. These models are based on action of several internal forces generated by the mass elements and center-mass of a top. The action of a top's weight produces its own internal torques that interrelate and act at one time and expresses precession motions. A top rotating eccentric center-mass manifests a nutation process. The obtained mathematical models for the top's motions enable describing physical principles of acting forces. These models of motions for a well-balanced top allowed its minimal angular velocity for self-stabilization to be defined. The diagram of a top's nutation represents the motions of the top with eccentricity of its center-mass. The new mathematical models for the motions of the well-balanced top and with eccentricity of its center-mass definitely respond to the practical results.

5. Discussion

New studies of the gyroscope effects have shown that the origin of the acting forces and motions in a gyroscope is more complex. The gyroscope effects result from action of the several inertial torques generated by the centrifugal,

Coriolis, and common inertial forces as well as the change in the angular momentum of the spinning rotor. The action of the new internal torques clearly describes the physics of gyroscope's motions and changes the traditional presentation of gyroscope effects. This new study enables describing gyroscope properties that were unexplainable at former time. Today new mathematical models for acting internal torques can be applied to any gyroscopic devices and manually solve all technical problems. These new analytical solutions were applied for describing the forces acting on a well-balanced top and on a top with the eccentricity of center-mass. The new physical principles enabled formulating mathematical models of top processed motions, nutation, and its ability to rotate vertically.

6. Conclusion

In gyroscope theory, the top's motions are one of the most complex and intricate in terms of analytical solutions. Known mathematical models for the top motions are accepted with simplifications and do not adequately express a real picture of its motions. The new mathematical models for gyroscope torques consider the simultaneous and interdependent action of several inertial forces generated by the rotating mass of the spinning rotor. As a practical application, these new physical principles for gyroscope motions were used for modeling a top's motions that include micro oscillation and self-stabilization. These mathematical models are thus distinguishable from those in well-known publications, which tend to have complex numerical modeling that does not interpret the origin of gyroscope effects. The application of new mathematical models for the top's motions effectively and clearly demonstrates physical principles of acting forces and motions. In that regard, this is also a good example of educational processes.

Nomenclature

a_{ir}:	Linear motion along axis i, that is, a_x or a_y along axis ox or oy, respectively
$a_{i.\max}$; $a_{i.\min}$:	Maximal and minimal linear motion along axis i, respectively
g:	Gravity acceleration
F:	Centrifugal force
$F_{\mathrm{ct}.my}$:	Centrifugal force of a top toy's center-mass rotating around axis oy
i:	Index for axis ox or oy
J:	Mass moment of inertia of a top
J_i:	Mass moment of inertia of a top around axis i
l:	Length of a top's leg
m:	Mass of a top
T:	Load torque
$T_{\mathrm{am}.i}$, $T_{\mathrm{ct}i}$, $T_{\mathrm{cr}.i}$, $T_{\mathrm{in}.i}$:	Torque generated by the change in the angular momentum, centrifugal, Coriolis, and common inertial forces acting around axis i, respectively
$T_{r.i}$, T_{pi}:	Resistance and precession torque acting around axis i, respectively
T_{ex}, T_{ey}:	Torques generated by eccentricity of the center-mass and action around axes ox and oy, respectively
V_i:	Linear velocity along axis i
$V_{i.\max}$; $V_{i.\min}$:	Maximal and minimal value of the linear velocity along axis i, respectively
t:	Time
α:	Angle for calculating the maximal value of the torques' magnitude
γ:	Tilt angle of a top's axis
ω:	Angular velocity of a top
ω_i:	Angular velocity of precession around axis i
$\omega_{i.\max}$; $\omega_{i\,\min}$:	Maximal and minimal value of the angular velocity of precession around axis i, respectively.

Conflicts of Interest

The authors declare that they have no conflicts of interest.

References

[1] F. Dell'Olio, T. Tatoli, C. Ciminelli, and M. N. Armenise, "Recent advances in miniaturized optical gyroscopes," *Journal of the European Optical Society: Rapid Publications*, vol. 9, Article ID 14013, 2014.

[2] G. Greenhill, *Report on Gyroscopic Theory*, Ein Dienst der ETH-Bibliothek ETH, Zürich, Schweiz, 2017.

[3] J. B. Scarborough, *The Gyroscope Theory and Applications*, Nabu Press, London, UK, 2014.

[4] Q. Hu, Y. Jia, and S. Xu, "Adaptive suppression of linear structural vibration using control moment gyroscopes," *Journal of Guidance, Control, and Dynamics*, vol. 37, no. 3, pp. 990–996, 2014.

[5] J. Li, M.-G. Suh, and K. Vahala, "Microresonator Brillouin gyroscope," *Optica*, vol. 4, no. 3, pp. 346–348, 2017.

[6] R. C. Hibbeler, *Engineering Mechanics - Statics and Dynamics*, Prentice Hall, Pearson, Singapore, 13th edition, 2015.

[7] K. Russell, Q. Shen, and R. S. Sodhi, *Kinematics and Dynamics of Mechanical Systems: Implementation in MATLAB® and SimMechanics®*, CRC Press Taylor and Francis Group LLC, Boca Raton Fl, USA, 2016.

[8] S. H. H. Kachapi and D. D. Ganji, *Dynamics and Vibrations: Progress in Nonlinear Analysis*, Solid Mechanics and its Applications, Springer Dordrecht Heidelberg, London, UK, 2014.

[9] S. Askari, M. H. Asadian, K. Kakavand, and A. M. Shkel, "Vacuum sealed and getter activated MEMS Quad Mass Gyroscope demonstrating better than 1.2 million quality factor," in *Proceedings of the 3rd IEEE International Symposium on Inertial Sensors and Systems, ISS 2016*, pp. 142-143, USA, February 2016.

[10] L. Gu and Z. Gan, "Phase conjugate fiber optic gyroscope," *Journal of Lightwave Technology*, vol. 32, no. 9, Article ID 6750014, pp. 1663–1668, 2014.

[11] I. Pasciuto, G. Ligorio, E. Bergamini, G. Vannozzi, A. M. Sabatini, and A. Cappozzo, "How angular velocity features and different gyroscope noise types interact and determine orientation estimation accuracy," *Sensors*, vol. 15, no. 9, pp. 23983–24001, 2015.

[12] T. Su, S. Nitzan, P. Taheri-Tehrani, M. Kline, B. Boser, and D. A. Horsley, "Silicon MEMS disk resonator gyroscope with an integrated cmos analog front-end," *IEEE Sensors Journal*, vol. 14, no. 10, 2014.

[13] B. Edamana, Y. Chen, D. Slavin, E. E. Aktakka, and K. R. Oldham, "Estimation with Threshold Sensing for Gyroscope Calibration Using a Piezoelectric Microstage," *IEEE Transactions on Control Systems Technology*, vol. 23, no. 5, pp. 1943–1951, 2015.

[14] M. Glueck, D. Oshinubi, and Y. Manoli, "Automatic real-time offset calibration of gyroscopes," *Microsystem Technologies*, vol. 21, no. 2, pp. 429–443, 2014.

[15] M. Häußler, R. Reichart, A. Bartl, and D. J. Rixen, "Post correcting for gyroscopic effects via dynamic substructuring," in *Proceedings of the 24th International Congress on Sound and Vibration, ICSV 2017*, July 2017.

[16] D. Senkal, A. Efimovskaya, and A. M. Shkel, "Minimal realization of dynamically balanced lumped mass WA gyroscope: Dual Foucault pendulum," in *Proceedings of the 2nd IEEE International Symposium on Inertial Sensors and Systems, IEEE ISISS 2015*, USA, March 2015.

[17] Z. Mohammadi and H. Salarieh, "Investigating the effects of quadrature error in parametrically and harmonically excited MEMS rate gyroscopes," *Measurement*, vol. 87, pp. 152–175, 2016.

[18] S. A. Zotov, I. P. Prikhodko, B. R. Simon, A. A. Trusov, and A. M. Shkel, "Self-calibrated MEMS gyroscope with AM/FM operational modes, dynamic range of 180 dB and in-run bias stability of 0.1 deg/hr," in *Proceedings of the Inertial Sensors and Systems – Symposium Gyro Technology*, Karlsruhe, Germany, September 2014.

[19] F. Klein and A. Sommerfeld, *The Theory of the Top*, vol. I-IV, Springer, Birkhäuser, New York, NY, USA, 2008-2014.

[20] W. Gander, M. J. Gander, and F. Kwok, *Scientific Computing - An Introduction using Maple and MATLAB*, Texts in Computational Science and Engineering, Springer, London, UK, 2014.

[21] R. Usubamatov, "Mathematical model for gyroscope effects," in *Proceedings of the AIP Conference*, vol. 1661, American Institute of Physics, 2015.

[22] R. Usubamatov, "Gyroscope internal kinetic energy and properties," *International Journal of Advancements in Mechanical and Aeronautical Engineering*, vol. 3, pp. 16–20, 2016.

[23] R. Usubamatov, "A mathematical model for motions of gyroscope suspended from flexible cord," *Cogent Engineering*, vol. 3, no. 1, Article ID 1245901, 2016.

[24] R. Usubamatov, "Mathematical models for principles of gyroscope theory," in *Proceedings of the AIP Conference*, pp. 020133-1–020133-21, 2017.